Nano Energy 86 (2021) 106080

Contents lists available at ScienceDirect

Nano Energy

journal homepage: www.elsevier.com/locate/nanoen

Review

Development and outlook of high output piezoelectric nanogenerators

Qi Xu, Juan Wen, Yong Qin *

Institute of Nanoscience and Nanotechnology, School of Materials and Energy, Lanzhou University, Lanzhou 730000, China

ARTICLE INFO

Keywords:
Nanogenerator
Piezoelectric nanogenerator
Power extraction circuit
Mechanism
Polarization rotation
Energy harvesting

ABSTRACT

With the rapid development of the Internet of things (IoT), wearable electronics, how to power them has been a great challenge, as the traditional powering method via batteries suffers from the problems of batteries' limited capacity and lifetime. Piezoelectric nanogenerators (PENGs) is one of the most promising solutions, as they can convert the ubiquitous and versatile mechanical energy into electricity. Since its invention in 2006, the PENG has achieved tremendous progress. Its voltage has increased from a few millivolts to hundreds of volts, and its current has increased from nanoampere to hundreds of microamperes. In this review, the working mechanisms of PENGs are discussed at first to point out how to improve PENGs' output theoretically. Then, according to the theoretical analysis, concrete methods including developing piezoelectric materials with high electromechanical response, structural optimization to scale up the electricity generated by individual nanomaterials are discussed. Next, considering the mismatch between the pulse signal generated by PENGs and the stable power supply requirement for conventional electronics, power extraction circuits are discussed. Finally, an outlook of future developments of high output PENGs is given.

1. Introduction

With the rapid advancement of semiconductor industry and microelectronics, the emerged functional devices such as implantable medical devices, personal wearable electronics, and the Internet of things (IoT) have reached every corner and played important roles in daily life [1,2]. For example, the smartwatch can be used to monitor heart rate to protect overall health; IoT can help people live and work comfortably and easily, and push forward the development of industry and agriculture. Currently, powering these devices mainly rely on rechargeable batteries. Due to limited capacity and lifetime, batteries need be constantly monitored, recharged and replaced, which will put the patients under a high risky surgical procedure for the implantable devices, be very frustrating and impractical in the work environment for wearable devices, be infeasible for the IoT due to the widely distributed nodes [3]. Fortunately, there are abundant energies in the environment and biomechanical movement. It is thus desirable to harvest these energies into electricity to prolong the lifetime of the above-mentioned devices or even get rid of the batteries by forming self-powered systems [4–19].

Ambient energy sources such as solar, [20–22] radio frequency, [23–25] temperature gradient, [26–28] kinetic energy [29–32] has been widely studied for energy harvesting and gained intensive attention. Among them, the kinetic energy is ubiquitous and versatile. It can come from *in-vivo* like heartbeat, diaphragmatic movement; human activities such as walking, typing; movements in environment including fluid flow generated by wind, water and so on. The kinetic energy in the environment shares some common characters: the amplitude and frequency of the mechanical energy source in the environment are usually random, weak and low. Although the traditional piezoelectric transducers have been used for mechanical energy harvesting for a long time, [32–34] they are not appropriate for the above-mentioned environment kinetic energy harvesting. On one hand, once the mechanical vibrating frequency is deviated from the resonant frequency of the piezoelectric transducer, the energy conversion efficiency of the piezoelectric transducer will decrease severely; on the other hand, conventionally, the kinetic energy in the environment is too weak to drive the bulk piezoelectric material used in the piezoelectric transducers. Since its invention, [29] piezoelectric nanogenerator (PENG) has attracted much attention, as it can convert tiny ambient irregular kinetic energy into electricity via the piezoelectric nanomaterials. Till now, big progresses have been made during PENGs' development. The electricity generated by the PENG can be used to directly lighten commercial LEDs in real-time [35]. Moreover, by combing PENGs with functional devices, self-powered systems can be constructed to realize maintenance-free and sustainable operation. Self-powered systems for UV sensing, [6] Hg^{2+} ion detection, [4] blood pressure monitoring [36] have been

* Corresponding author.
E-mail address: qinyong@lzu.edu.cn (Y. Qin).

https://doi.org/10.1016/j.nanoen.2021.106080
Received 9 March 2021; Received in revised form 14 April 2021; Accepted 15 April 2021
Available online 23 April 2021

demonstrated, respectively. In above applications of PENGs, improving PENGs' output is important, otherwise, either additional energy storage unit or high precision measurement should be provided.

In order to improve PENGs' output, many works referring to materials selection, innovative device designs, structural integrations et al., have been done. The output voltage of the nanogenerator has increased from a few millivolts to hundreds of volts, and the output current has increased from nanoamperes to hundreds of microamperes (Fig. 1). So, it is necessary to give an overview about these works and provide a rational route towards developing PENGs with higher output in the future. This paper first reviews the key ideas of the published works for improving PENGs' output in a systematic way. Section 2 briefly presents the theory of PENGs. Section 3 discusses on how to improve the PENGs' output from the material point of view. Section 4 discusses on how to improve the PENGs' output from the structural point of view. Section 5 discusses on how to extract the power generated by the PENG maximally by the electric circuits. Finally, we give a short summary about this review and an outlook about the future development of high output PENGs.

2. Working mechanism of PENGs

The PENGs work by converting the mechanical energy into electricity through the piezoelectric effect. The piezoelectric effect is governed by the underlying constitutive equations,

$$\begin{cases} \sigma_p = c_{pq}\varepsilon_q - e_{kp}E_k \\ D_i = e_{iq}\varepsilon_q + \kappa_{ik}E_k \end{cases} \quad (1)$$

where E_k is the electric field, D_i is the electric displacement, σ_p is the stress tensor, ε_p is the strain tensor, c_{pq} is the elastic modulus tensor, e_{kp} is the piezoelectric tensor, κ_{ik} is the dielectric tensor. Eq. (1) is a set of coupled equations, where electric field and mechanical deformation are tangled up. Solving this equation is a tedious process and analytic solution doesn't exist conventionally. Gao et al. [37] used a perturbation expansion method to handle the coupled equation, and obtained an analytic expression of the piezoelectric potential distribution within a first order approximation for the PENG (Fig. 2a–i) deflected by an AFM tip. From the comparison between the approximated analytic result and the result obtained by solving the coupled equation with the finite element method (Fig. 2a-ii, iii, iv), the difference between them is smaller than 6%, which shows the accuracy of this perturbation expansion method. In this process, a new concept remnant displacement D_{Ri} was proposed. As showed in Eqs. (2) and (3), through D_{Ri}, the generated body charge ρ^R and surface charge Σ^R of the piezoelectric material are related to the external force induced strain ε_p. Based on the above information, the mechanism of the PENGs can be stated as follows: under external force, the generated body charge and surface charge of the piezoelectric material will induce a potential drop across the electrodes of the PENG; once the PENG is connected to the external load, the potential drop will drive the electrons flow to generate electricity.

$$D_{Ri} = e_{ip}\varepsilon_p \quad (2)$$

$$\begin{cases} \rho^R = -\dfrac{\partial D_{Ri}}{\partial x_i} \\ \Sigma^R = n_i D_{Ri} \end{cases} \quad (3)$$

As shown in Eq. (2), the electric displacement D_R is decided by both strain and piezoelectric tensor. According to Eq. (3), if the strain distributes uniformly inside the piezoelectric materials, only the remnant surface charge exists. In this case, the PENG can be considered as a charged capacitor. The equivalence circuit of the PENG can be considered as a voltage source V_O connected in serial with a capacitor C_P (Fig. 2b) [38]. The voltage source is given by Eq. (4),

$$V_O = \frac{e_{ip}\varepsilon_p}{C_P} \quad (4)$$

where C_{PENG} is the capacitance of the PENG. When the PENG is connected to a load, there will be some voltage drop across the C_P, so the output voltage will be smaller than the open circuit voltage. As shown in Fig. 2b, the C_P and external load make up a first order high pass passive RC filter. The cut-off frequency f_0 is equal to $1/(2\pi RC_P)$. Conventionally, this frequency is much larger than the working frequency of PENGs especially for the single nanowire based PENGs due to the small capacitance of the nanowire. So, the voltage across the external load attenuated severely. As indicated by Xu et al. [38] from a theoretical

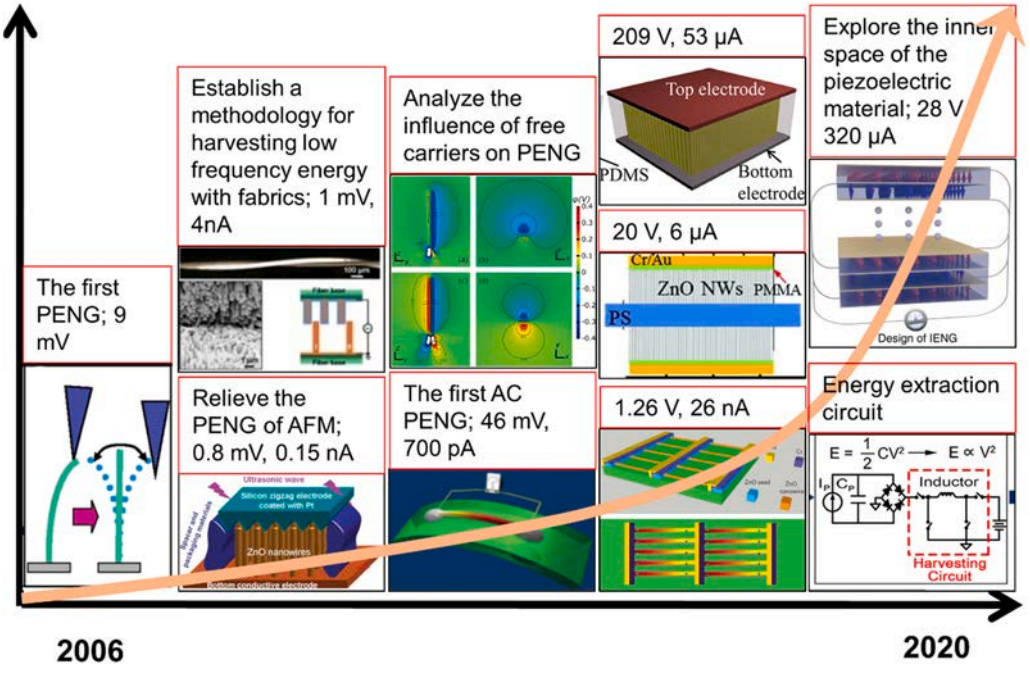

Fig. 1. The development of high output nanogenerators [29,35,119–122,125,130,132,133].

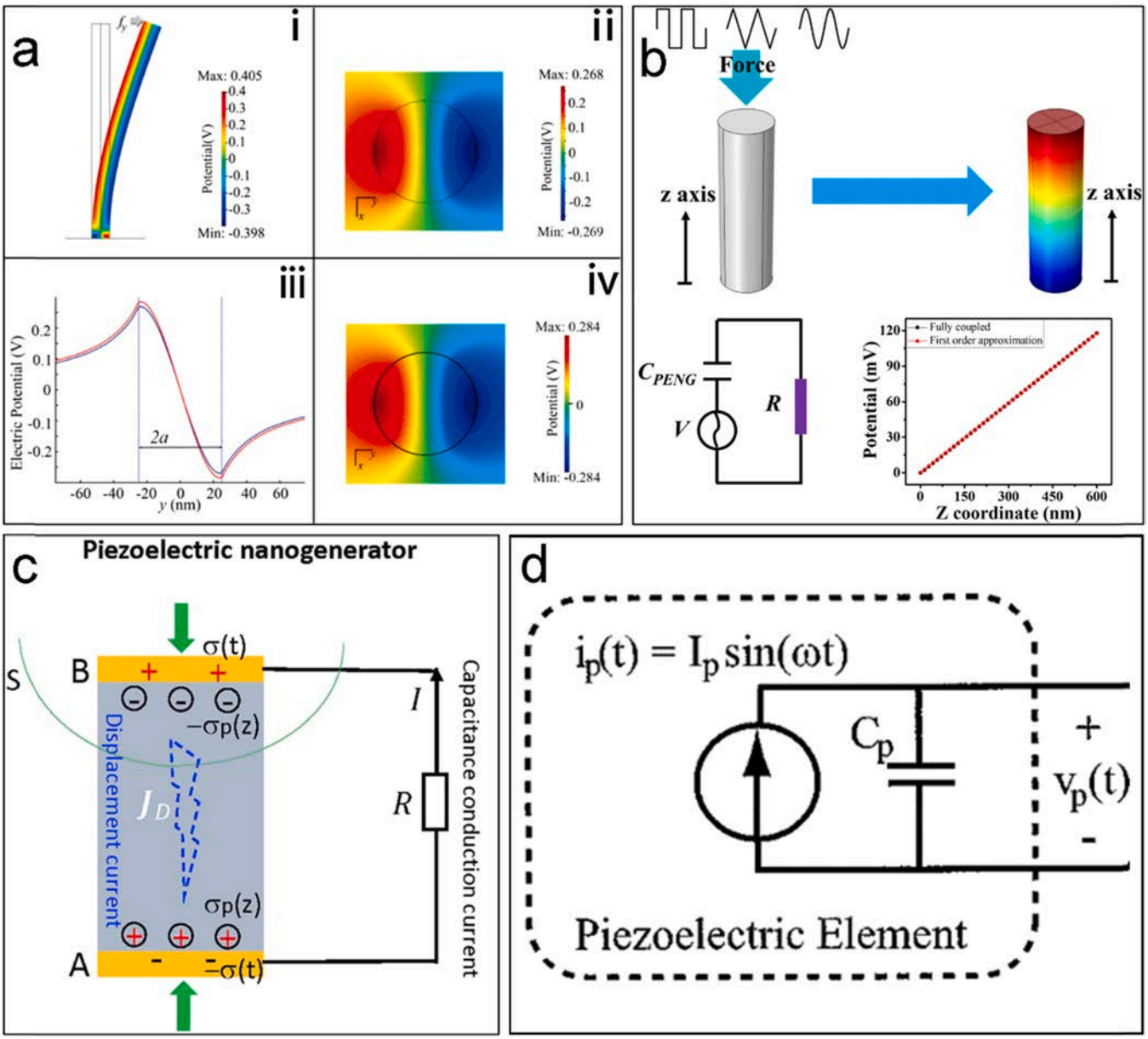

Fig. 2. Different models of PENG. (a) i. The distribution of piezoelectric potential of a deflected nano wire (length 600 nm,diameter 50 nm) under a lateral force of 80 nN; Cross sectional (z0 = 300 nm) piezoelectric potential of the PENG calculated by finite element method (ii) and analytic solution (iii). iv. Comparation of the piezoelectric potential calculated by the above two methods [37]. (b) The equivalent circuit of a PENG where the PENG is considered as a voltage source [38]. (c) The displacement currentin a PENG [40]. (d) The equivalent circuit of a PENG where the PENG is considered as a current source [41].

study, as for a PZT-5 H nanowire (length 500 nm, radius 25 nm) based PENG driven by harmonic force, the voltage (73.1 nV) across a 100 MΩ external load will attenuated by nearly six orders compared with the open-circuit voltage (118 mV), and found that under low frequencies, the square formed force is more advantageous for powering electronics with small resistance.

Later, Wang et al. [39,40] found it is the displacement current (Fig. 2c) that drives the conversion from mechanical energy into electricity. The displacement current density is given by Eq. (5),

$$J = \frac{\partial D_R}{\partial t} = e_{ip}\frac{\partial \varepsilon_p}{\partial t} \tag{5}$$

In this case, the equivalence circuit of the PENG can be considered as a current source i_p connected in parallel with a capacitor C_P (Fig. 2d) [41]. In the circuit analysis, either current source or voltage source can be used, and the voltage source can be converted into current source by Norton's theorem. Eq. (5) relate the strain rate, piezoelectric coefficient to the output of PENG. The faster strain rate and higher piezoelectric coefficient will lead to a larger output of PENG. From the equivalent circuit, it can be seen during the working of PENG, a portion of the charge will be stored in C_P and can't be delivered into the external load. So, given fixed strain rate and device area, which are conventionally constrained by the working environment, improving the piezoelectric coefficients of piezoelectric materials, enlarging the current density of the PENGs, and designing electric circuit to extract the power generated by PENGs are effective ways toward high output PENGs.

3. Material aspect

At the end of Section 2, we pointed out increasing the piezoelectric coefficient is one way to improve the PENGs' output. With the development of PENGs, there are three categories of piezoelectric materials

that attracted researchers' attention. The first is ceramic ferroelectrics such as lead zirconate titanate (PZT), [42–44] lead magnesium niobate titanate (PMN-PT), [45,46] barium titanate (BTO), [47,48] sodium potassium niobite (KNN), [49,50] sodium bismuth titanate (NBT) [51,52]. This kind of materials has high piezoelectric coefficient especially for lead-containing materials [53] such as PZT, PMN-PT. The second kind of materials is the ferroelectric polymers and ferroelectric composites. Compared with the ceramic ferroelectrics, although their piezoelectric coefficient is small, they are more compatible with the current processing technologies [54,55] and suitable for medical applications [56, 57] and wearable electronics [58–60] due to the flexibility and non-toxic property. The last kind material is the semiconducting piezoelectric materials such as ZnO, [29] GaN, [61,62] CdS [63]. This kind of materials are not only ferroelectric materials but also semiconducting materials, and they can be further applied in piezotronics [64]. These three kinds of materials have their own application scenarios, and in this section, we will give a briefly introduction for each kind.

3.1. Ceramic ferroelectrics

The ferroelectric materials have a non-zero spontaneous polarization which can be reversed under the applied external electric field. Among the ferroelectric materials, the perovskite-type materials are famous for the large piezoelectric constants. Some studies show that the ultrahigh electromechanical response of the perovskite-type ferroelectrics comes

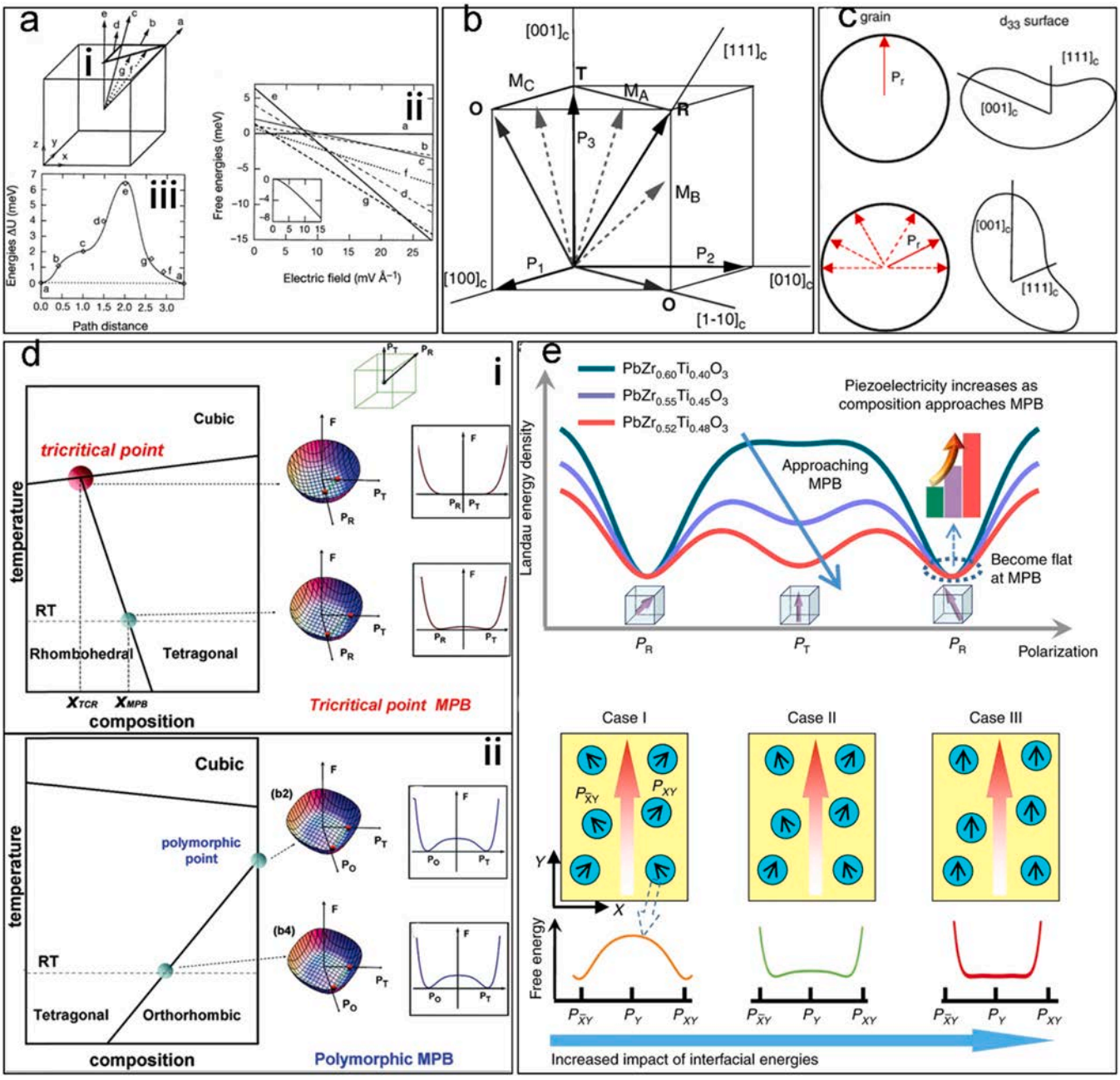

Fig. 3. Methods to improve the piezoelectric performance of ceramic ferroelectrics. (a) The free energy of BTO with different polarization directions [134]. (b) Polarization in the cubic system and rotation path between different phases [71]. (c) The d_{33} surface for rhombohedral ceramics with different remnant polarization direction [71]. (d) Schematic of a tricritical-type MPB, (i) the corresponding free energy surface at the tricritical point and MPB composition at room temperature. Schematic of a polymorphic-type MPB, (ii) the corresponding free energy surface at the polymorphic point and MPB composition at room temperature [76]. (e) Schematics about increasing the piezoelectric coefficient by introducing local structural heterogeneity [80].

from polarization rotation [65–68]. Fu et al. [69] analyzed this phenomenon from the first principle study. The BTO was selected to be the research object due to its simple structure compared with solid solutions such as PZT. Different polarization directions as shown in Fig. 3a–i are considered. From the relations between the free energy of BTO and external electric field (Fig. 3a-ii), with the increase of external electric field, the minimum free energy path corresponds to a rotation of polarization from a to e along the a→f→g→e path. The calculated d_{33} of this path will be 5 times larger than that of the other path (a→b→c→d→e). The internal energy of BTO with different polarization directions (Fig. 3a-iii) was calculated to analyze this big difference in d_{33}. Compared with the two paths from a to e, the energy surface of the path a→f→g→e is more flat, which means the polarization will rotate easier along this path under external disturbance than the other path, and thus lead to a large d_{33}. In addition, polarization rotation alone can lead to a giant d_{33} of 293 pC/N, which confirms the important role played by polarization rotation. It should be noted that, the maximum electromechanical response is not along the polar directions conventionally [70]. Take BTO as an example, the polar direction is along [111] c as shown in Fig. 3b, in order to rotate the polarization, the external disturbance should be applied off this direction. The direction along which possesses maximum electromechanical response can be determined from the expression of longitudinal piezoelectric constant d^*_{33} [71].

$$d^*_{33}(\theta) = \cos\theta\left(d_{15}\sin^2\theta + d_{31}\sin^2\theta + d_{33}\cos^2\theta\right) \tag{6}$$

$$d_{15} = \varepsilon_0\chi_{11}Q_{44}P_3 \tag{7}$$

$$d_{33} = 2\varepsilon_0\chi_{33}Q_{11}P_3 \tag{8}$$

where θ is the angle between the [001] axis and the desired direction, d_{15} is the shear piezoelectric constant, Q_{11} and Q_{44} are the electrostrictive constants, χ_{11} and χ_{33} are the dielectric susceptibilities along and perpendicular to the spontaneous polarization P_3, respectively. As for PZT ceramics near the morphotropic phase boundary (MPB) region, due to the large value of the shear piezoelectric constant d_{15}, the maximum d_{33} lie with an angle about 45–60° with respect to the polar axis. So, as shown in Fig. 3c, the PZT ceramics with polar axis deviated 45–60° from normal direction of electrode will have larger electromechanical response than the case where the polar axis is perpendicular to the electrode.

In order to facilitate polarization to improve piezoelectric materials' electromechanical response, a flat free energy surface is needed to decrease the barrier during the rotation process. To realize this, there are several ways. One of them is to construct regions where several phases coexist such as tuning the compositions of PZT to MPB region [72,73]. Conventionally, the polarization direction is constrained by symmetry, which goes against the polarization rotation. However, near the MPB, due to the coexist of phases, the polarization can rotate from one phase to another phase via their common symmetry element. A typical material among the perovskite ferroelectric is $PbZr_{1-x}Ti_xO_3$ (PZT). Near the MPB region, which separates tetragonal structure and rhombohedral structure in the phase diagram, the PZT has the highest piezoelectric constant about 500 pC/N [74]. The emerged monoclinic phase (M) provide a bridge between the two phases through the common symmetry element, the pseudocubic (110) mirror plane [75]. In this mirror plane the thermodynamic energy connecting the tetragonal and rhombohedral phases is flattened, the local polarizations can be rotated from $< 111 >$ to $< 001 >$ directions under external electric or mechanical stimuli and thus lead to a large piezoelectric constant. Conventionally, compared with the PZT family, the non-Pb piezoelectric materials' piezoelectricity is inferior. Liu et al. [76] found that the reason is due to the difference between two MPB types. The PZT has a tricritical-type MPB (Fig. 3d-i), at the tricritical point, the polarization anisotropy vanish and the polarization can rotate from $< 111 >$ R to $< 001 >$ T freely. As for most of the non-Pb piezoelectric materials, they have a polymorphic MPB (Fig. 3ᴅ-ii), there is no restriction to the polarization anisotropy, so the polarization from $< 111 >$ R to $< 001 >$ T will experience a large barrier and show an inferior piezoelectricity compared with PZT family. Besides constructing multiphase coexisting regions, introducing structural heterogeneity is another way to improve ceramic ferroelectric's electromechanical response. With the discovery of relaxor-PT materials, researchers found that their piezoelectric constants are even higher. In this kind of materials featured by diffuse ferroelectric transitions, the polarization is correlated in the nanoscale to form many polar nanoregions (PNRs). Inside these PNRs, the symmetry is lowered, however, as a whole the symmetry of the relaxor ferroelectrics is the same as the paraelectric phase [77]. In the microscopic point of view, the formation of PNRs is related to the composition disorders. Using a dynamic pair-density function method, Dmowski et al. [78] found that the PNRs of $Pb(Mg_{1/3}Nb_{2/3})O_3$ are formed by hybridization p-orbital of Pb and O, where Pb is off-centered toward Mg^{2+} more than Nb^{5+} to form local rhombohedral distortion. Li et al. [79] found that the introduced interfacial energy due to the PNRs can flatten the Landau energy can thus facilitate the polarization rotation. Later, by doping Sm into the $Pb(Mg_{1/3}Nb_{2/3})O_3$-$PbTiO_3$ and introducing nanoscale structural heterogeneity (Fig. 3e), a piezoelectric constant d_{33} up to 1500 pc/N is obtained [80].

3.2. Ferroelectric polymers and ferroelectric composites

Compared with ceramic piezoelectric materials, ferroelectric polymers and ferroelectric composites are lightweight, flexible and are complementary to the ceramic ferroelectrics. Among the ferroelectric polymers, PVDF is one representative material. It should be noted that different from the conventional piezoelectric materials, the longitudinal piezoelectric coefficient of PVDF and its copolymer with trifluoroethylene (P(VDF-TrFE)) are both negative [81]. As shown in Fig. 4a, a negative longitudinal piezoelectric coefficient means that when an electric field is exerted along the c-axis of the materials, unlike the conventional materials, the PVDF will experience a contraction. Therefore, the PVDF is not suitable for the matrix to form ferroelectric composites with ceramic ferroelectrics. Due to the similar radius between H (1.2 Å) and F (1.35 Å) atom, PVDF has five phases which are α-PVDF, β-PVDF, γ-PVDF, δ-PVDF, and ε-PVDF. Among these phases, the α-PVDF is stable and easy to be acquired during the polymerization process, β-PVDF has the outstanding ferroelectric properties due to the alignment of $-CF_2CH_2$-base units perpendicular to the polymeric chain. So, in order to improve PVDF's electromechanical performance, we should increase the content of β phase in PVDF. Till now, many methods have been developed to increase the β phase content. Sencadas et al. [82] studied the influence of stretching ratio and temperature on the formation of phase. Under a stretching ratio of 500% and temperature of 80 °C, the β phase content increased to 80%. However, a decrease of crystallinity about 10% was accompanied. Meng et al. [83] developed a press and folding (P&F) method to improve the β phase content. The P&F cycle is composed of a folding process and a subsequent pressing lasting 5 min with 300 kN under 165 °C, then the cold water is used to quench the system with the pressing force maintained. After 7 such cycles, the β phase content has been increased to 98%, which can be ascribed to the effective stress transfer during the P&F cycle compared with the uniaxial mechanical stretching. Besides the direct mechanical stretching and pressing, the extensional force experienced by the polymer jet during the electrospinning can also facilitate the formation of β phase, in addition, the high voltage exerted between the syringe tip and the collector can pole the electrospun fiber [84,85]. Polymerizing PVDF by adding other monomer, to form P(VDF-TrFE), [86,87] P(VDF-HFP) [88] copolymer can also improve the β phase content. The P(VDF-TrFE) is a kind of polymer relaxor ferroelectric. Different from the atomic disorder induced inorganic relaxor ferroelectrics, in P(VDF-TrFE) the relaxor behavior originates from conformational

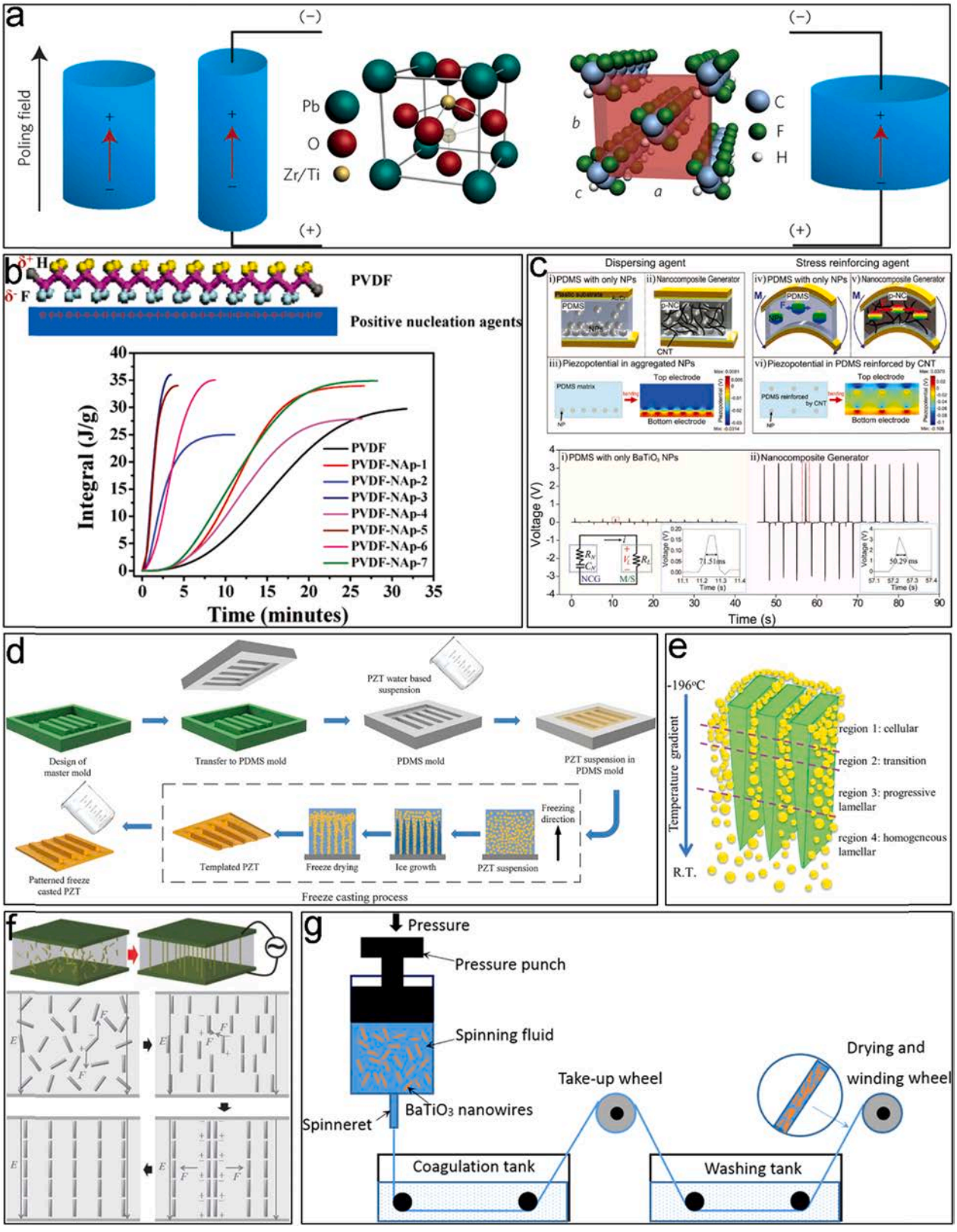

Fig. 4. Methods to improve the piezoelectric performance of polymer and composite. (a) The structure of β phase PVDF, and counterintuitive behavior under poling field with respect to PZT [81]. (b) Schematic of interaction between PVDF and nucleation agents, and integral isothermal crystallization differential scanning calorimetry curves of PVDF with different content of nucleation agents [97]. (c) Schematics of BTO/PDMS composite, calculated piezoelectric potential distribution, and tested output voltage of PENG with and without dispersing agent, respectively [98]. (d) Schematics of synthesizing interconnected PZT in PDMS by freeze cast method [100]. (e) Schematic of the gradient PZT ceramic [101]. (f) Well aligned PZT nanowires in PDMS by dielectrophoresis [104]. (g) The fabricating process of single fiber BTO nanowires/PVC composite by spinning process [105].

disorder discovered by Liu et al. [89] The asymmetric carbon atom in TrFE brings chain chirality to P(VDF-TrFE). Owing to the chain chirality, in ground state, the P(VDF-TrFE) has a 3/1-helical conformation. The distortion of the gauche torsional angles triggered the disorders of 3/1-helical conformation and give birth to the relaxor behavior of P (VDF-TrFE). The epitaxy process can improve the crystallinity and piezoelectric performance of P(VDF-TrFE). Park et al. [90] spin coated P (VDF-TrFE) solution on PTFE followed by heat treatment at 135 °C for 2 h. Due to the lattice matched faces between $(010)_{P(VDF\text{-}TrFE)}$ and $(100)_{PTFE}$, edge-on crystalline lamellae of P(VDF-TrFE) lying on the substrate was obtained and the crystallinity reached 70%. Jung et al. [91] increased the crystallinity of a spin coated P(VDF-TrFE) to 60% by applying a static shear force during the heat treatment, where narrow crystalline lamellae grown perpendicular to the shear direction. The electrical polarization was enhanced by 50%. In this method, additional interlayer such as PTFE is not needed, and the P(VDF-TrFE) can be spin coated on any substrate. Besides shearing force, applying a pressing force with a removable PTFE template during the heat treatment, the obtained epitaxy P(VDF-TrFE) shows an enhanced d_{33} of − 40.7 pC/N in contrast to the − 20–30 pC/N of nonepitaxial film. This performance enhancement can be ascribed to the formation of edge-on lamellae structure due to the limited segmental motion of P(VDF-TrFE) under dimensional confining [92]. However, the polarization is weakened due to the less electric polarity of the monomer compared with -CH_2-CF_2- unit [93]. So, there exist a balance between the increased β phase content and decreased polarization in the copolymers. By adding fillers [94–96] into PVDF, with the aid of interactions between the -CH_2-CF_2- and filler surface (Fig. 4b), the -CF_2CH_2- will align along the polymer chain to improve the β phase content [97]. Manna et al. [95] used ester functionalized multiwalled carbon nanotubes (F-MWNT) to promote β phase content of PVDF. The interaction of the carbonyl group in the ester with CF_2 group of PVF_2, initiate the nucleation in β phase and the subsequent growth process is promoted by the interaction of PVF_2 with the F-MWNT surface. By tuning the concentration of F-MWNT in PVF_2 to 2%, a pure (100%) β phase can be obtained from a solvent-cast process.

Ferroelectric composites consist of nano ceramic ferroelectrics and polymer matrix possess both the polymer's flexibility and the ceramic materials' high piezoelectric performance. Just like ferroelectric polymers, the ferroelectric composite is also suitable for implantable medical devices and wearable electronics. Due to the large surface energy of nanomaterials and the sticky property of polymer matrix, the nano ceramic ferroelectrics tend to aggregate in the polymer matrix. As shown in Fig. 4c, if the BTO nanoparticles aggregate on the bottom, the generated piezoelectric potential is smaller than that of the even distributed case [98]. So, how to disperse the nanomaterials evenly in the polymer matrix and avoid aggregation is important. One way to improve the dispersion of nanomaterials is adding fillers. Park et al. used the graphic carbons to improve the dispersion of BTO nanoparticles in PDMS [98]. With the addition of graphic carbons, the BTO nanoparticles can disperse evenly by attaching themselves to the graphic carbons formed scaffold. Later, metal nanowires were used to replace graphic carbons, as compared with graphic carbons, the self-interactions between metal nanowires are weak, which is more advantageous to improve the dispersion of nanomaterials [99]. Beside dispersing ferroelectric fillers evenly in the polymer matrix, enhancing the connectivity of fillers is also important. Composite with interconnected structured ferroelectric fillers can solve the problem of insufficient polarization of fillers due to the large permittivity mismatch between the ceramic fillers and polymer matrix, and promote the stress transfer from polymer matrix to fillers [100,101]. The stress is transferred from polymer matrix to filler through the interfacial shear stress. If the filler length is too short, the stress transfers between fillers will reduce the effective modulus of filler material [102]. When a dynamic force is applied, the fillers should keep a long length to realize complete stress transfer [103]. So, longer filler will contribute to the stress transfer from polymer matrix to fillers. To improve the piezoelectric material's connectivity in polymer matrix, Xie et al. used a freezing cast method to enable PZT nanoparticles form dendritic PZT channels in PDMS matrix as shown in Fig. 4d [100]. Besides the connected channel, the flexure of the dendritic PZT caused by the lateral expansion of PDMS under compression also contribute to the improvement of the composite's piezoelectric performance. Later, Liu et al. found that the PZT fillers fabricated by the freeze cast method has a gradient structure and are composed of cellular region, transition region, progressive lamellar region and homogeneous lamellar region as shown in Fig. 4e [101]. Applying stress to these regions and testing the generated output voltage and current from them, respectively, they found the progressive lamellar region shows the maximum electric output, as this region has a higher concentration of PZT ceramics compared with homogeneous lamellar region and more effective channel for stress transfer compared with cellular region, transition region. The dispersion of nanomaterials can also be improved by external factors. Hu et al. improved the dispersion of PZT nanowires in PDMS by dielectrophoresis [104]. As shown in Fig. 4e, after electric field is exerted across the electrodes, randomly distributed PZT nanowires will rotate along the electric field, and then align in columns due to attraction force caused by the opposite charge induced in head and tail of adjacent PZT nanowires, and finally the columns repel each other due to the repulsive forces and evenly dispersed PZT nanowire arrays in PDMS are formed. Zhang et al. used a spinning method to align the BTO nanowires in polyvinylchloride (PVC) fibers [105]. As shown in Fig. 4f, the original randomly distributed PZT in PVC will become aligned in the final composite fiber due to the large shear force during the spinning process. The 3D printing approach is a state-of-the-art technology for creating piezoelectric architectures with complex structures and high resolution. To solve the contradiction between the piezoelectric performance which need high loading content of piezoelectric ceramics and processability which need low loading content of piezoelectric ceramics, Chen et al. [106] added de-binding and sintering processes during the 3D printing of $BaTiO_3$, and a density corresponds to 93.47% of the bulk materials was obtained. Compared with conventional materials fabricating technique, the 3D printing technique has more freedom to tune spatial arrangement of materials, Cui et al. [107] analyzed the electric displacement maps of different 3D node units, based on which the effective piezoelectric constant can be custom designed, and directionality sensing was realized by 4 designed 3D node units. An in-situ poling was introduced in the 3D printing. Recently, Li et al. [108] developed an electric field-assisted 3D printing technology for piezoelectric materials, during the printing process the piezoelectric materials can be poled simultaneously, which avoids poling failure of large complex print. Based on this technology, an artificial artery system based tubular sinusoidal architecture of $K_{0.5}Na_{0.5}NbO_3$@PVDF are printed, this artery showed a high sensitivity of 0.306 mV/mmHg.

As for ferroelectric composites, the Maxwell-Wagner interfacial polarization arising from the charge accumulation on interface between fillers and polymer matrix with different permittivity and conductivity, will lead to a large dielectric constant due to the increased overall polarization [109]. Based on the interfacial polarization between poly (2,2, 2-trifluoroethyl methacrylate) (PTF) and PDMS, Kim et al. designed a triboelectric nanogenerator (TENG) with a high k friction layer, and a 4.9 times enhancement of triboelectric charge density is obtained. As for PENG, large dielectric constant is bad for the performance improvement. High dielectric constant will increase the capacitance of the PENG, deduced from the equivalent circuit of PENG as shown in Fig. 2d, more portion of displacement current will flow into the capacitor and decrease the power delivered to the external circuit. As for the metal fillers, the high conductivity of metal will lead to a complex permittivity of composite [110], and a portion of power generated by PENG will be dissipated.

3.3. Semiconducting piezoelectric materials

Different from the above two kinds of piezoelectric materials,

piezoelectric semiconducting materials possess free carriers which will influence the PENG's output performance [111]. A large carrier density will screen the immobile piezoelectric charges and decrease the output voltage of the PENG. Decreasing the free carriers is one solution to increase the PENG's output. Lee et al. demonstrate that by constructing a pn junction between the n-type ZnO and the p-type polymer poly (3-hexylthiophene) (P3HT) as shown in Fig. 5a. During the establish of pn junction, the free carriers in ZnO will be extracted to the P3HT side, through which the free carriers in ZnO are decreased, and an 18 times increase in output voltage was obtained [112]. Besides decreasing the free carriers, the same as ceramic ferroelectrics, improving the piezoelectric coefficient is important to achieve large electromechanical response for semiconducting piezoelectric materials. Among the II-VI semiconductors such as ZnO, ZnS, CdS, and III-V semiconductors such as GaN, GaAs, AlN, the ZnO has the highest piezoelectric coefficient. In general, the piezoelectric coefficient consists of a clamped ion term and an internal strain term. These two terms are opposite in sign. As for ZnO, the cancellation between the piezoelectric coefficient generated by these two terms is the least and the piezoelectric coefficient is dominated by the internal strain term [113]. In order to improve the electromechanical response of ZnO, it needs to understand its microscale origin firstly. As shown in Fig. 5b, the variation of the bond length of Zn_2-O_2 colinear with the *c* axis is thought to be main reason for the electromechanical response of ZnO. However, Karanth et al. found that when an electric field is applied along the *c*-axis, the slop of variation of projection length Zn_2-O_1 along *c*-axis (0.610 $Å^2$/V) is over 2 times larger than the slop of variation of the length of Zn_2-O_2 (0.278 $Å^2$/V), which demonstrate that the electromechanical response should mainly come from the rotation of Zn_2-O_1 [114]. Unlike the case of ceramics such as PZT, where the total polarization rotates under applied field, the direction of total polarization of ZnO is unchanged throughout the rotation of Zn_2-O_1. Based on above analysis, facilitating the rotation of Zn_2-O_1 bond is one way to increase the electromechanical response of ZnO. Luo et al. found that if the Zn^{2+} in ZnO is substituted by transition metal dopant with smaller radius than Zn^{2+} (Fig. 5c), the piezoelectric coefficient can be enhanced due to the easier rotation of transition metal ion-oxygen bonds (Fe^{3+}-O_1 as shown in Fig. 5c) compared with the zinc-oxygen bonds [115]. Compared with the d_{33} of undoped ZnO film, after doping a concentration of 1.2 at% Fe into ZnO, the d_{33} of doped ZnO film can be enhanced to 127 pC/N. Zhang et al. found that when halogen dopants with radius larger than oxygen were doped into ZnO, the dopants induced tensile strain was beneficial to ZnO based PENGs to improve their output [116]. Later, Choi et al. used an in-situ method to study the influence of strain engineering on the electromechanical response of ZnO [117]. When a tensile strain is exerted along the *c*-axis, the off-centered displacement of Zn (Fig. 5d-i, ii) will contribute to an increase in the spontaneous polarization along the c-axis. As shown in Fig. 5D-iii, when the strain changes from 0% to 4.87%, the spontaneous polarization increases from 0.062 to 0.095 μC/m^2. The increased spontaneous polarization leads to an 270% improvement of piezoelectric coefficient. Besides the piezoelectric coefficient, the elastic limit is also crucial to piezoelectric materials. Materials with higher elastic limit can endure larger elastic strain during PENG's working process. In order to improve the piezoelectric materials' elastic limit, Kim et al. fabricated a truss-like 3D hollow ZnO structure with a shell thickness of 100 nm by combing 3D nanolithography and atomic layer deposition (ALD) [118]. The structure has an elastic limit of 10% in contrast to the elastic limit of 3% about fully filled ZnO due to the geometrically improved critical buckling stability and decreased flaw size constrained by the nanostructure.

4. Structure optimization

Apart from selecting materials with high piezoelectric coefficients, structural optimization is also one important way to improve the PENG's output. The first PENG was composed of an atomic force microscope (AFM) with Pb coated tip and grounded ZnO nanowire arrays (Fig. 6a) [29]. When the AFM tip is in contact with the tensile side of the nanowire during the scanning process, the negatively biased Schottky contact between the AFM tip and the nanowire will hinder the electron flow into the ZnO nanowire. When the AFM tip located to the compressive side of the nanowire, the Schottky contact is positive biased, and the electrons in the nanowire will pour out of the nanowire and a signal (9 mV) will be detected in the external load. Later, Wang et al. used a Pb coated Zigzag silicon electrode (Fig. 6b) to replace the Pb coated AFM tip to liberate PENG from dependence on expensive and heavy AFM instrument [119]. In this design a large number of nanowires can be deflected simultaneously, different from the pulsed signal generated by the AFM aided PENG, the output signal of this PENG driven by ultrasonic waves is more continuous. Besides, Qin et al. intertwined two fibers grown with radially ZnO nanowire arrays and formed a teeth-to-teeth interface, one of the ZnO nanowire arrays were coated with Au which played the role of AFM tips [120]. The teeth-to-teeth interface can guarantee more ZnO nanowires involved for producing electricity. By pulling one fiber back and forth with relative to the other fiber, the PENG output a voltage of 1 mV and a current of 4 nA. In the above designs, the PENGs worked by deflecting the nanowire arrays laterally, during which, the piezoelectric potential is distributed across the cross section of the nanowire and its magnitude is proportional to the cubic of the nanowire's diameter [37]. Due to small size of the nanowire's diameter, the output voltage is hard to improve.

To solve the above problems, Yang et al. developed an alternating current (AC) PENG [121]. As shown in Fig. 6c, a ZnO microwire was placed on a plastic substrate, with its two ends formed Ohmic and Schottky contact respectively. Upon bending the substrate, a tensile strain will be introduced in the axial direction of the ZnO nanowire. By bending the substrate back and forth, the PENG output a voltage of 46 mV and a current of 700 pA. In this design, the ends of the nanowire are tightly bonded to the electrodes which improve the PENG's robustness. Moreover, different from the DC PENGs, the piezoelectric potential is along the axial direction of the nanowire, which will lead to a large voltage drop across the electrodes and thus lead to a higher output voltage. Finally, compared with the DC PENG, this PENG is easier to integrate. As for the semiconducting piezoelectric material ZnO, under external force, the sign of the output voltage depends on the directions of *c*-axis. So, in integrating ZnO nanowires, the *c*-axis of the nanowires should toward the same one direction to avoid the cancellation of the output generated by individual nanowires. Xu et al. [122] made a PENG by lateral growing ZnO nanowires on a ZnO strip-like seed pattern through a hydrothermal method. Firstly, arrays of ZnO seed strip are fabricated on a Kapton film. Secondly, the top surface and one side surface are covered with Cr layer, so the ZnO nanowire can only grow on the left side surface. After the growth, each row has about 2000 nanowires, by integrating 700 such rows, a PENG with output of 1.2 V and 26 nA was obtained. For the hydrothermal method, the crystal quality of ZnO nanowires are limited due to the low grow temperature (< 100 ℃) and usually possess high free carrier density [123]. Later, Zhu et al. used a sweep-printing-method to transfer the nanowire arrays grown on silicon substrate via chemical vapor deposition method on a plastic substrate [124]. Applying a shear force between the silicon and the receiving flexible substrate, the nanowires will detach from the silicon substrate and align uniformly toward one direction to ensure the orientation consistency of *c*-axis on the flexible substrate (Fig. 6d). After that, stripped electrodes are patterned on the flexible substrate by photolithography method to connect these aligned nanowires together, a PENG with output of 2.03 V and 107 nA was obtained. To reduce the adverse effect brought about by excess free carriers, Hu et al. deposited the as-grown ZnO nanowire arrays with positively charged polymer poly (diallydimethylammonium chloride) (PDADMAC) and negatively charged poly (sodium 4-styrenesulfonate) (PSS) in sequence to passivate the ZnO nanowire surface and decrease the free carrier density, and a PENG with output of 20 V and 6 μA was obtained [125]. Zhu et al.

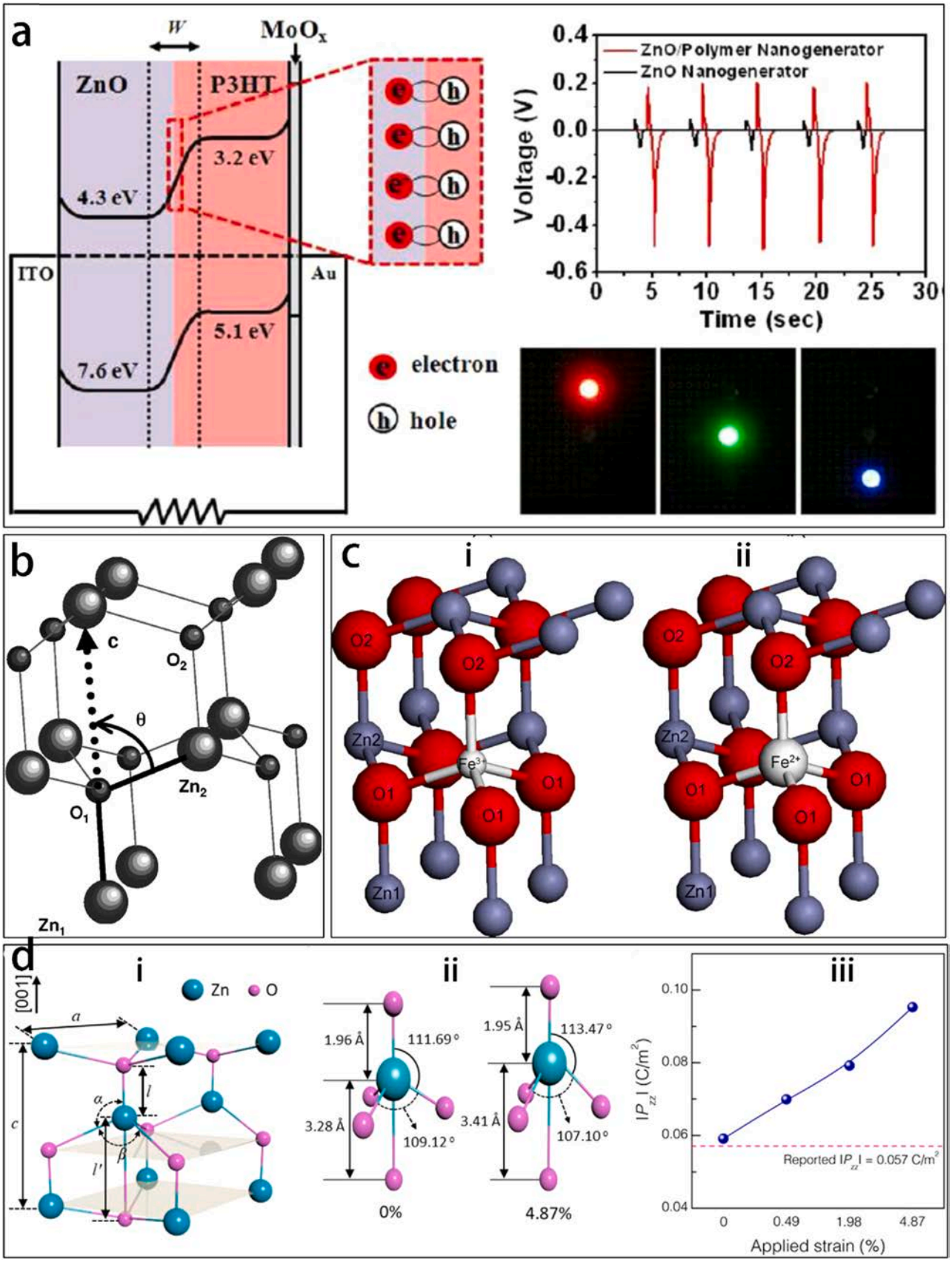

Fig. 5. Methods to improve the piezoelectric performance of semiconducting piezoelectric materials. (a) Schematic of the band edge alignment and the output of the PENGs [112]. (b) The structure of wurtzite ZnO [114]. (c). Supercell of the Fe^{3+} and Fe^{2+} doped ZnO system [115]. (d). Schematics of structural change of the ZnO under applied strains (i) and the variation of spontaneous of polarization with applied strains (ii) [117].

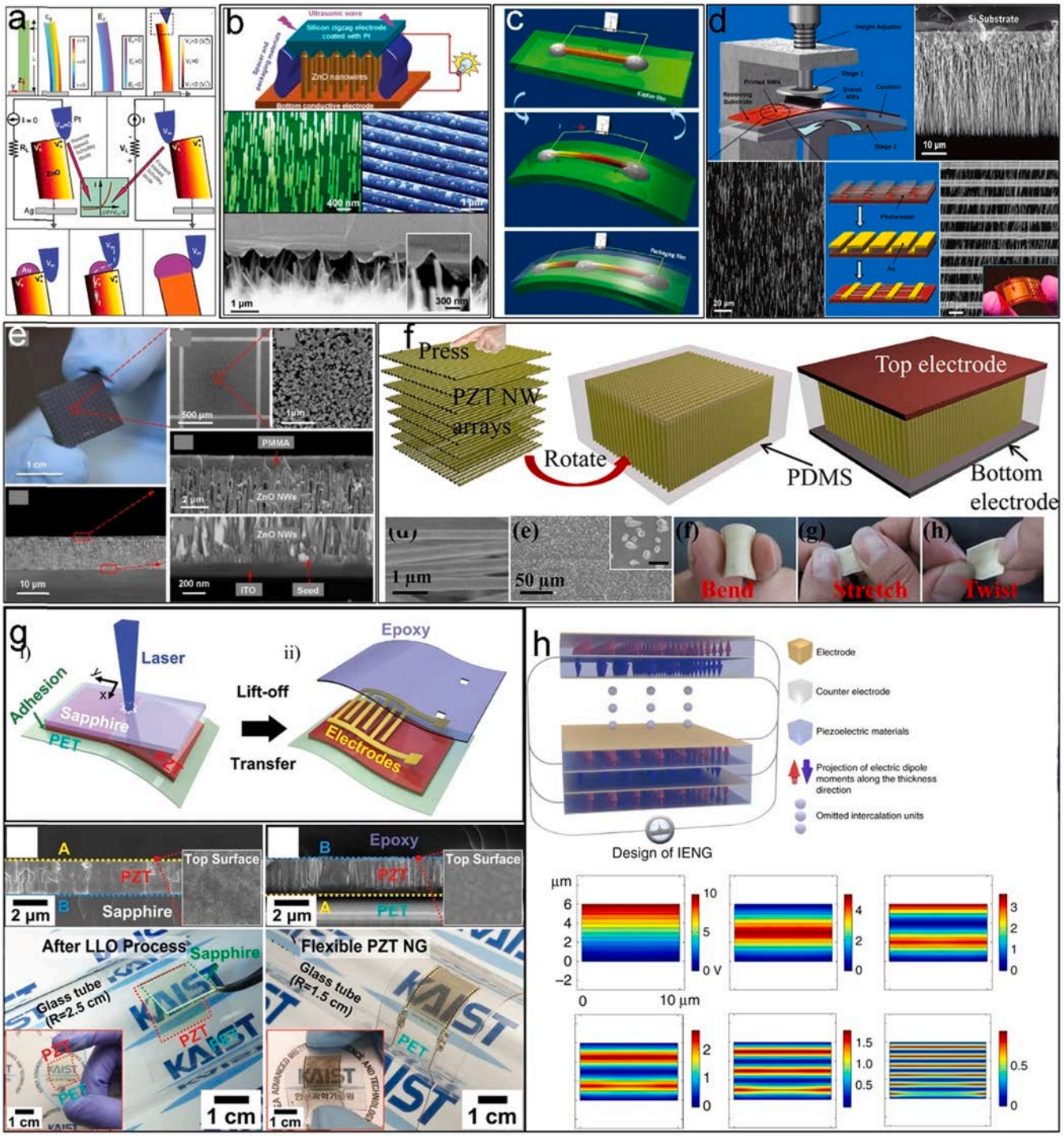

Fig. 6. Improving the output of PENG by structural optimization. (a) The first PENG invented in 2006 [29]. (b) Increasing the amount of involved nanowire by replacing the AFM tip with zigzag electrode coated with Pt [119]. (c) The first AC PENG invented in 2009 [121]. (d) Integrating nanowires detached from nanowires arrays on a flexible substrate. (e) Structure of the PENG composed of densely nanowire arrays [126]. (f) Schematic fabricating process and the structure of PENG by vertical integration of ultralong aligned electronspun fibers [35]. (g) Schematic fabricating process and structure of PZT thin film PENG based on interdigitated electrodes [129]. (h) Schematic fabricating process and piezoelectric potential distribution of the PENG based on three-dimensional intercalation electrodes [130].

selectively grown dense nanowire arrays on the silicon substrate (Fig. 6e) [126]. After that, a thin layer of PMMA layer was spin-coated on the top layer of nanowire arrays. This thin layer plays the role of Schottky contact. Compared with the Schottky contact, the barrier height between the electrode and ZnO nanowire arrays is large, which can effectively decrease the leakage current and improve the PENG's output. This PENG has a voltage of 58 V, a current of 134 μA. Given a fixed strain, the piezoelectric potential is proportional to the nanowire's length. So, increasing the nanowire's length is an effective way to improve PENGs' output. Among the various methods of synthesizing nanowires such as hydrothermal, chemical vapor deposition, electrospinning is advantageous in preparing long fibers, by which tens of centimeters of aligned fibers can be fabricated [127]. Gu et al. developed a novel structure by vertically integrating ultralong aligned electrospun

fibers to improve the PENG's output (Fig. 6f) [35]. Firstly, film composed of aligned ultralong fibers was synthesized by suspending sintering technique [128]. Secondly, the films were stacked layer by layer and then stuck together by dilute PDMS. After excluded the redundant PDMS, and solidified, a PENG with voltage of 209 V and current of 53 μA was obtained.

At that time, the voltage generated by PENGs has been large enough to drive daily electronics. However, their current is too low. To increase the current, Park et al. [129] developed a PZT thin film based PENG (Fig. 6g). Firstly, a thin layer of PZT with 2 μm thickness was deposited on the sapphire substrate by multiple sol-gel processes. Then the PZT film on the sapphire substrate was transferred to a PET substrate via a laser lift-off (LLO) process. Followed by a fabrication of Au interdigitated electrodes, the PENG was fabricated. By bending the substrate back and forth, a PENG with voltage of 200 V and current density of 150 μA/cm^2 was obtained. As for the interdigitated electrodes, only part of the piezoelectric material can be utilized for power generation, as the area beneath the interdigitated electrodes is short circuited. Although

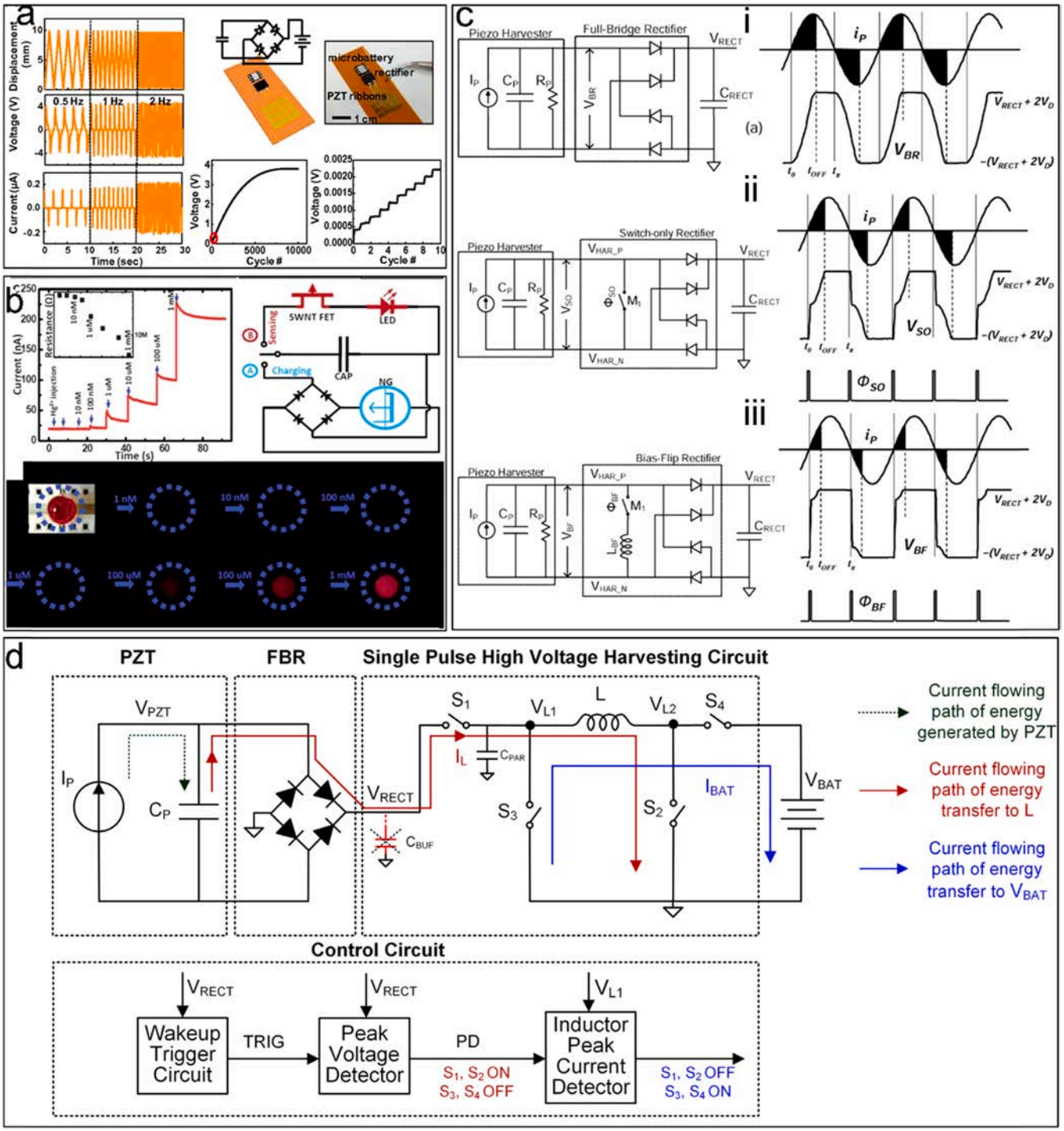

Fig. 7. Circuits for extracting the power generated by PENG. (a) Output of a PZT ribbon-based PENG and the voltage on the cointegrated micro battery during PENG's operating process [4]. (b) Photograph of Hg^{2+} sensor and a self-powered Hg^{2+} detecting system [4]. (c) Switch-only rectifier, bias-flip rectifier and the corresponding associated current and voltage signals [131]. (d) Block diagram for the energy extraction enhancement circuit [132].

the covered area by interdigitated electrodes can be reduced via adopting narrower electrode strips, the accompanying new problems of insufficient materials polarization comes. To solve this problem, Gu et al. put forward a three-dimensional intercalation electrode as shown in Fig. 6h [130]. By embedding intercalation electrode into piezoelectric material, the piezoelectric materials can be fully utilized, and the piezoelectric materials can be fully polarized due the uniformly distributed electric field across the adjacent electrodes. By constructing 6 pairs of such layered electrodes, the PENG can output current of 320 μA, which corresponds to a current density 290 μA/cm^2.

5. Power extraction circuit for nanogenerator

Due to the randomness of the ambient mechanical energy, the generated output by the PENG is not regular and is pulsed signal. This kind of output can't be directly used to power conventional electronics. So, a power extraction circuit is needed to match the power generated by PENGs with conventional electronics. The usually used power extraction circuit is the full-bridge rectifier. After regulated by the full-bridge rectifier, the electricity generated by PENGs is stored in rechargeable batteries (Fig. 7a) or capacitors (Fig. 7b). To improve the power extraction efficiently, Ramadass et al. analyzed different rectifiers and proposed an inductor-based bias-flip rectifier scheme, whose power extraction capability is four times larger than the conventional full-bridge rectifiers [131]. As for the full-bridge rectifier (Fig. 7c–i), when the voltage across the capacitor is lower than the output voltage V_{RECT}, the diodes are reverse biased, no current will flow to the external load, and the current will charge the capacitor C_P. When the voltage V_{BR} is bigger than V_{RECT}, the diode is positive biased, the current starts to flow to the external load, till the current decreases to zero. The shade portion represent the amount of charge which can't flow into the external load every cycle. Due to the shade portion of the charge, the power extraction efficiency is only 12.5% for the full-bridge rectifier. Fig. 7c-ii is a switch-only rectifier, every time when the current becomes zero, the switch M1 is turn on to discharge the C_P till the C_P is completely discharged. By this way, the work needed to do in the positive half-cycle is greatly reduced. Albeit, the work must be done to charge the capacitor from 0 to V_{RECT}. To improve the power extraction efficiency further, apart from a switch M1, an inductor is also connected in parallel with the capacitor C_P to form a bias-flip rectifier (Fig. 7c-iii). When the current i_p becomes zero, the switch is turned on. The capacitor C_P and the inductance L make up an LC resonant circuit. With the aid of inductor, the voltage sign on the capacitor can be flipped in an interval of $2\pi(LC)^{1/2}$, when the sign of the voltage across the capacitor is flipped, the switch M1 is turned off. Now only a bit work needs to be done to increase the flipped voltage to V_{RECT}, and the charge generated by the piezoelectric energy harvester can flow into the external load mostly. Later, Khan et al. get rid of the capacitor and used an inductor to transfer the energy generated by the PENG [132]. As shown in Fig. 7d, all switches are turned off initially. Till the voltage across C_P is larger than a threshold V_{THRS}, S1 and S2 are tuned on, the energy stored in C_P is transferred in the inductor L. After the energy is totally transferred in L, S1 and S2 are turned off, S3 and S4 are turned on in the meantime, the energy stored in L is transferred into the battery. Through this design, the harvested energy increases to 408% compared with the energy harvested by full-bridge rectifier.

6. Summary and outlook

This paper gives an overview about the recent advances of high output PENGs. The working mechanism of PENGs is discussed, and the importance of displacement current has been highlighted. Based on the expression of displacement current and the equivalent circuit of PENGs, the previous works on improving PENGs' output are divided into three categories: materials aspect, structure aspect and power extraction circuit aspect. Developing materials with high piezoelectric coefficient is a prerequisite for high output PENGs. For various application scenarios, different kinds of materials are needed. Methods toward improving the piezoelectric coefficient for each kind of materials are discussed, respectively. For the ceramic ferroelectrics, flattening the Landau energy and facilitating the polarization rotation is an effective way to improve the materials' piezoelectric coefficient. As for the ferroelectric polymers and ferroelectric composites, improving the ferroelectric β phase content of PVDF is important. In addition, for ferroelectric composite, increasing the dispersion of ceramics to avoid aggregation is beneficial for the improvement of the composite's electromechanical response. As for the semiconducting piezoelectric materials, they possess free carriers, which can screen part of the generated piezoelectric potential generated under external stimuli. So, apart from improving the intrinsic materials' piezoelectric coefficient, the density of free carriers should also be reduced to achieve better electromechanical response. After discussing the material aspect, in the structure optimization, designs toward improving the output voltage as well was output current are discussed. Finally, the irregular and peak signal can't be directly used for powering daily electronics and power extraction circuit is needed to match the power generated by PENGs with conventional electronics, and the evolution of power extraction circuit is presented. By applying dynamic switches and inductors, the extracted energy from PENGs has increased largely.

Albeit the big process has been achieved these years, there is still space to improve the PENGs' output further. Firstly, the piezoelectric coefficient of ferroelectric polymers is too low compared with ceramic ferroelectrics. Besides PVDF and its copolymer, new type of polymer ferroelectrics is need to be explored. Secondly, the previous works mainly focused on materials, structural part, and circuit designs, the strain rate is seldom researched. From Eq. (5) in Section 2, the strain rate is closely related to the displacement current. Although, the mechanical stimuli in the environment is irregular, the mechanical stimuli may be modulated to improve the PENGs' output by special mechanical designs.

Author Contributions

Yong Qin conceived the structure of this review. Qi Xu, Juan Wen and Yong Qin wrote the manuscript. Yong Qin, Qi Xu and Juan Wen revised the manuscript.

Declaration of Competing Interest

The authors declare that they have no known competing financial interests or personal relationships that could have appeared to influence the work reported in this paper.

Acknowledgements

We sincerely acknowledge the support from the Joint Fund of Equipment Pre-research and Ministry of Education, China (No. 6141A02022518), the National Program for Support of Topnotch Young Professionals, China the Fundamental Research Funds for the Central Universities, China (No. lzujbky-2020-sp08), the Natural Science Basic Research Plan in Shaanxi Province of China (2019JQ-652).

References

[1] S.M.R. Islam, D. Kwak, M.H. Kabir, M. Hossain, K.-S. Kwak, The internet of things for health care: a comprehensive survey, Ieee Access 3 (2015) 678–708.
[2] A. Zanella, N. Bui, A. Castellani, L. Vangelista, M. Zorzi, Internet of things for smart cities, IEEE Internet Things J. 1 (2014) 22–32.
[3] Z. Watral, A. Michalski, Selected problems of power sources for wireless sensors networks, IEEE Instrum. Meas. Mag. 16 (2013) 37–43.
[4] M. Lee, J. Bae, J. Lee, C.-S. Lee, S. Hong, Z.L. Wang, Self-powered environmental sensor system driven by nanogenerators, Energy Environ. Sci. 4 (2011) 3359–3363.

[5] C.F. Pan, Z.T. Li, W.X. Guo, J. Zhu, Z.L. Wang, Fiber-based hybrid nanogenerators for/as self-powered systems in biological liquid, Angew. Chem. -Int. Ed. 50 (2011) 11192–11196.
[6] S. Bai, Q. Xu, L. Gu, F. Ma, Y. Qin, Z.L. Wang, Single crystalline lead zirconate titanate (PZT) nano/micro-wire based self-powered UV sensor, Nano Energy 1 (2012) 789–795.
[7] C.F. Pan, W.X. Guo, L. Dong, G. Zhu, Z.L. Wang, Optical fiber-based core-shell coaxially structured hybrid cells for self-powered nanosystems, Adv. Mater. 24 (2012) 3356–3361.
[8] Y. Jie, N. Wang, X. Cao, Y. Xu, T. Li, X. Zhang, Z.L. Wang, Self-powered triboelectric nanosensor with poly(tetrafluoroethylene) nanoparticle arrays for dopamine detection, ACS Nano 9 (2015) 8376–8383.
[9] S. Lee, R. Hinchet, Y. Lee, Y. Yang, Z.H. Lin, G. Ardila, L. Montes, M. Mouis, Z. L. Wang, Ultrathin nanogenerators as self-powered/active skin sensors for tracking eye ball motion, Adv. Funct. Mater. 24 (2014) 1163–1168.
[10] G.-T. Hwang, H. Park, J.-H. Lee, S. Oh, K.-I. Park, M. Byun, H. Park, G. Ahn, C. K. Jeong, K. No, H. Kwon, S.-G. Lee, B. Joung, K.J. Lee, Self-powered cardiac pacemaker enabled by flexible single crystalline pmn-pt piezoelectric energy harvester, Adv. Mater. 26 (2014) 4880–4887.
[11] H.L. Zhang, Y. Yang, T.C. Hou, Y.J. Su, C.G. Hu, Z.L. Wang, Triboelectric nanogenerator built inside clothes for self-powered glucose biosensors, Nano Energy 2 (2013) 1019–1024.
[12] H. Zhang, Y. Yang, Y. Su, J. Chen, C. Hu, Z. Wu, Y. Liu, C.P. Wong, Y. Bando, Z. L. Wang, Triboelectric nanogenerator as self-powered active sensors for detecting liquid/gaseous water/ethanol, Nano Energy 2 (2013) 693–701.
[13] Y. Yang, H.L. Zhang, Y. Liu, Z.H. Lin, S. Lee, Z.Y. Lin, C.P. Wong, Z.L. Wang, Silicon-Based Hybrid Energy Cell for Self-Powered Electrodegradation and Personal Electronics, Acs Nano 7 (2013) 2808–2813.
[14] Y. Yang, H.L. Zhang, J. Chen, S.M. Lee, T.C. Hou, Z.L. Wang, Simultaneously harvesting mechanical and chemical energies by a hybrid cell for self-powered biosensors and personal electronics, Energy Environ. Sci. 6 (2013) 1744–1749.
[15] Y. Yang, H.L. Zhang, J. Chen, Q.S. Jing, Y.S. Zhou, X.N. Wen, Z.L. Wang, Single-electrode-based sliding triboelectric nanogenerator for self-powered displacement vector sensor system, Acs Nano 7 (2013) 7342–7351.
[16] Z.-H. Lin, G. Zhu, Y.S. Zhou, Y. Yang, P. Bai, J. Chen, Z.L. Wang, A self-powered triboelectric nanosensor for mercury ion detection, Angew. Chem. -Int. Ed. 52 (2013) 5065–5069.
[17] P. Lin, X. Yan, Z. Zhang, Y. Shen, Y. Zhao, Z. Bai, Y. Zhang, Self-powered UV photosensor based on PEDOT:PSS/ZnO micro/nanowire with strain-modulated photoresponse, ACS Appl. Mater. Interfaces 5 (2013) 3671–3676.
[18] A. Yu, P. Jiang, Z.L. Wang, Nanogenerator as self-powered vibration sensor, Nano Energy 1 (2012) 418–423.
[19] C. Xu, C.F. Pan, Y. Liu, Z.L. Wang, Hybrid cells for simultaneously harvesting multi-type energies for self-powered micro/nanosystems, Nano Energy 1 (2012) 259–272.
[20] M.A. Green, A. Ho-Baillie, H.J. Snaith, The emergence of perovskite solar cells, Nat. Photonics 8 (2014) 506–514.
[21] G. Li, R. Zhu, Y. Yang, Polymer solar cells, Nat. Photonics 6 (2012) 153–161.
[22] J.Y. Kim, J.-W. Lee, H.S. Jung, H. Shin, N.-G. Park, High-efficiency perovskite solar cells, Chem. Rev. 120 (2020) 7867–7918.
[23] I. Krikidis, S. Timotheou, S. Sasaki, RF energy transfer for cooperative networks: data relaying or energy harvesting? IEEE Commun. Lett. 16 (2012) 1772–1775.
[24] H.C. Sun, Y.X. Guo, M. He, Z. Zhong, A dual-band rectenna using broadband yagi antenna array for ambient rf power harvesting, IEEE Antennas Wirel. Propag. Lett. 12 (2013) 918–921.
[25] X. Zhang, J. Grajal, M. Lopez-Vallejo, E. McVay, T. Palacios, Opportunities and challenges of ambient radio-frequency energy harvesting, Joule 4 (2020) 1148–1152.
[26] R. Venkatasubramanian, E. Siivola, T. Colpitts, B. O'Quinn, Thin-film thermoelectric devices with high room-temperature figures of merit, Nature 413 (2001) 597–602.
[27] L.E. Bell, Cooling, heating, generating power, and recovering waste heat with thermoelectric systems, Science 321 (2008) 1457–1461.
[28] L. Sigrist, N. Stricker, D. Bernath, J. Beutel, L. Thiele, Thermoelectric energy harvesting from gradients in the earth surface, Ieee Trans. Ind. Electron. 67 (2020) 9460–9470.
[29] Z.L. Wang, J.H. Song, Piezoelectric nanogenerators based on zinc oxide nanowire arrays, Science 312 (2006) 242–246.
[30] F.R. Fan, Z.Q. Tian, Z.L. Wang, Flexible triboelectric generator!, Nano Energy 1 (2012) 328–334.
[31] H. Li, C. Tian, Z.D. Deng, Energy harvesting from low frequency applications using piezoelectric materials, Appl. Phys. Rev. 1 (2014), 041301.
[32] K.S. Ramadan, D. Sameoto, S. Evoy, A review of piezoelectric polymers as functional materials for electromechanical transducers, Smart Mater. Struct. 23 (2014), 033001.
[33] Q. Zhou, S. Lau, D. Wu, K. Shung, Piezoelectric films for high frequency ultrasonic transducers in biomedical applications, Prog. Mater. Sci. 56 (2011) 139–174.
[34] X. Dai, Y. Wen, P. Li, J. Yang, M. Li, Energy harvesting from mechanical vibrations using multiple magnetostrictive/piezoelectric composite transducers, Sens. Actuators A Phys. 166 (2011) 94–101.
[35] L. Gu, N. Cui, L. Cheng, Q. Xu, S. Bai, M. Yuan, W. Wu, J. Liu, Y. Zhao, F. Ma, Y. Qin, Z.L. Wang, Flexible fiber nanogenerator with 209 v output voltage directly powers a light-emitting diode, Nano Lett. 13 (2013) 91–94.
[36] X. Cheng, X. Xue, Y. Ma, M. Han, W. Zhang, Z. Xu, H. Zhang, H. Zhang, Implantable and self-powered blood pressure monitoring based on a piezoelectric thinfilm: Simulated, in vitro and in vivo studies, Nano Energy 22 (2016) 453–460.
[37] Y. Gao, Z.L. Wang, Electrostatic potential in a bent piezoelectric nanowire. The fundamental theory of nanogenerator and nanopiezotronics, Nano Lett. 7 (2007) 2499–2505.
[38] Q. Xu, Y. Qin, Function of JARID2 in bovines during early embryonic development, PeerJ 5 (2017), 4189.
[39] Z.L. Wang, On Maxwell's displacement current for energy and sensors: the origin of nanogenerators, Mater. Today 20 (2017) 74–82.
[40] Z.L. Wang, On the first principle theory of nanogenerators from Maxwell's equations, Nano Energy 68 (2020), 104272.
[41] G.K. Ottman, H.F. Hofmann, A.C. Bhatt, G.A. Lesieutre, Adaptive piezoelectric energy harvesting circuit for wireless remote power supply, IEEE Trans. Power Electron. 17 (2002) 669–676.
[42] N. Izyumskaya, Y. Alivov, S.J. Cho, H. Morkoc, H. Lee, Y.S. Kang, Processing, structure, properties, and applications of PZT thin films, Crit. Rev. Solid State Mater. Sci. 32 (2007) 111–202.
[43] G. Xu, Z.H. Ren, P.Y. Du, W.J. Weng, G. Shen, G.R. Han, Polymer-assisted hydrothermal synthesis of single-crystalline tetragonal perovskite PbZr0.52Ti0.48O3 nanowires, Adv. Mater. 17 (2005) 907–910.
[44] J. Wang, A. Durussel, C.S. Sandu, M.G. Sahini, Z. He, N. Setter, Mechanism of hydrothermal growth of ferroelectric PZT nanowires, J. Cryst. Growth 347 (2012) 1–6.
[45] S. Xu, G. Poirier, N. Yao, PMN-PT nanowires with a very high piezoelectric constant, Nano Lett. 12 (2012) 2238–2242.
[46] L. Bellaiche, D. Vanderbilt, Intrinsic piezoelectric response in perovskite alloys: PMN-PT versus PZT, Phys. Rev. Lett. 83 (1999) 1347–1350.
[47] H.X. Fu, L. Bellaiche, First-principles determination of electromechanical responses of solids under finite electric fields, Phys. Rev. Lett. 91 (2003), 057601.
[48] W.S. Yun, J.J. Urban, Q. Gu, H. Park, Ferroelectric properties of individual barium titanate nanowires investigated by scanned probe microscopy, Nano Lett. 2 (2002) 447–450.
[49] F. Rubio-Marcos, P. Marchet, T. Merle-Mejean, J.F. Fernandez, Role of sintering time, crystalline phases and symmetry in the piezoelectric properties of lead-free KNN-modified ceramics, Mater. Chem. Phys. 123 (2010) 91–97.
[50] F. Bortolani, A. del Campo, J.F. Fernandez, F. Clemens, F. Rubio-Marcos, High srain in (K,Na)NbO3-based lead-free piezoelectric fibers, Chem. Mater. 26 (2014) 3838–3848.
[51] Y. Hiruma, H. Nagata, T. Takenaka, Thermal depoling process and piezoelectric properties of bismuth sodium titanate ceramics, J. Appl. Phys. 105 (2009), 084112.
[52] Y.M. Chiang, G.W. Farrey, A.N. Soukhojak, Lead-free high-strain single-crystal piezoelectrics in the alkaline-bismuth-titanate perovskite family, Appl. Phys. Lett. 73 (1998) 3683–3685.
[53] P.K. Panda, B. Sahoo, PZT to lead free piezo ceramics: a review, Ferroelectrics 474 (2015) 128–143.
[54] X. Chen, X. Han, Q.-D. Shen, PVDF-based ferroelectric polymers in modern flexible electronics, Adv. Electron. Mater. 3 (2017), 1600460.
[55] M. Mai, S. Ke, P. Lin, X. Zeng, Ferroelectric polymer thin films for organic electronics, J. Nanomater. 2015 (2015) 1–14.
[56] X. Chen, J. Shao, N. An, X. Li, H. Tian, C. Xu, Y. Ding, Self-powered flexible pressure sensors with vertically well-aligned piezoelectric nanowire arrays for monitoring vital signs, J. Mater. Chem. C. 3 (2015) 11806–11814.
[57] F.S. Foster, E.A. Harasiewicz, M.D. Sherar, A history of medical and biological imaging with polyvinylidene fluoride (PVDF) transducers, Ieee Trans. Ultrason. Ferroelectr. Freq. Control 47 (2000) 1363–1371.
[58] W. Yang, W. Gong, C. Hou, Y. Su, Y. Guo, W. Zhang, Y. Li, Q. Zhang, H. Wang, All-fiber tribo-ferroelectric synergistic electronics with high thermal-moisture stability and comfortability, Nat. Commun. 10 (2019) 5541.
[59] S.K. Ghosh, D. Mandal, Synergistically enhanced piezoelectric output in highly aligned 1D polymer nanofibers integrated all-fiber nanogenerator for wearable nano-tactile sensor, Nano Energy 53 (2018) 245–257.
[60] Z.H. Liu, C.T. Pan, C.K. Yen, L.W. Lin, J.C. Huang, C.A. Ke, Crystallization and mechanical behavior of the ferroelectric polymer nonwoven fiber fabrics for highly durable wearable sensor applications, Appl. Surf. Sci. 346 (2015) 291–301.
[61] C.-Y. Chen, G. Zhu, Y. Hu, J.-W. Yu, J. Song, K.-Y. Cheng, L.-H. Peng, L.-J. Chou, Z.L. Wang, Gallium nitride nanowire based nanogenerators and light-emitting diodes, ACS Nano 6 (2012) 5687–5692.
[62] C.-T. Huang, J. Song, W.-F. Lee, Y. Ding, Z. Gao, Y. Hao, L.-J. Chen, Z.L. Wang, GaN nanowire arrays for high-output nanogenerators, J. Am. Chem. Soc. 132 (2010) 4766–4771.
[63] Y.-F. Lin, J. Song, Y. Ding, S.-Y. Lu, Z.L. Wang, Piezoelectric nanogenerator using CdS nanowires, Appl. Phys. Lett. 92 (2008), 022105.
[64] S. Liu, L. Wang, X. Feng, Z. Wang, Q. Xu, S. Bai, Y. Qin, Z.L. Wang, Ultrasensitive 2D ZnO piezotronic transistor array for high resolution tactile imaging, Adv. Mater. 29 (2017), 1606346.
[65] H. Liu, J. Chen, L.L. Fan, Y. Ren, Z. Pan, K.V. Lalitha, J.G. Rodel, X.R. Xing, Critical role of monoclinic polarization rotation in high-performance perovskite piezoelectric materials, Phys. Rev. Lett. 119 (2017), 017601.
[66] F.G. Wang, I. Grinberg, A.M. Rappe, Band gap engineering strategy via polarization rotation in perovskite ferroelectrics, Appl. Phys. Lett. 104 (2014), 152903.
[67] A.T. Mulder, N.A. Benedek, J.M. Rondinelli, C.J. Fennie, Turning ABO(3) antiferroelectrics into ferroelectrics: design rules for practical rotation-driven ferroelectricity in double perovskites and A(3)B(2)O(7) Ruddlesden-popper compounds, Adv. Funct. Mater. 23 (2013) 4810–4820.
[68] A. García, D. Vanderbilt, Electromechanical behavior of BaTiO3 from first principles, Appl. Phys. Lett. 72 (1998) 2981–2983.

[69] H. Fu, R.E. Cohen, Polarization rotation mechanism for ultrahigh electromechanical response in single-crystal piezoelectrics, Nature 403 (2000) 281–283.
[70] R. Zhang, B. Jiang, W. Cao, Single-domain properties of 0.67Pb(Mg1/3Nb2/3) O3–0.33PbTiO3 single crystals under electric field bias, Appl. Phys. Lett. 82 (2003) 787–789.
[71] D. Damjanovic, Contributions to the piezoelectric effect in ferroelectric single crystals and ceramics, J. Am. Ceram. Soc. 88 (2005) 2663–2676.
[72] F. Cordero, F. Trequattrini, F. Craciun, C. Galassi, Octahedral tilting, monoclinic phase and the phase diagram of PZT, J. Phys. Condens. Matter.: Inst. Phys. J. 23 (2011), 415901.
[73] M.R. Soares, A.M.R. Senos, P.Q. Mantas, Phase coexistence region and dielectric properties of PZT ceramics, J. Eur. Ceram. Soc. 20 (2000) 321–334.
[74] Y. Saito, H. Takao, T. Tani, T. Nonoyama, K. Takatori, T. Homma, T. Nagaya, M. Nakamura, Lead-free piezoceramics, Nature 432 (2004) 84–87.
[75] B. Noheda, J.A. Gonzalo, L.E. Cross, R. Guo, S.E. Park, D.E. Cox, G. Shirane, Tetragonal-to-monoclinic phase transition in a ferroelectric perovskite: the structure of PbZr0.52Ti0.48O3, Phys. Rev. B 61 (2000) 8687–8695.
[76] W. Liu, X. Ren, Large piezoelectric effect in pb-free ceramics, Phys. Rev. Lett. 103 (2009), 257602.
[77] V.V. Shvartsman, D.C. Lupascu, Lead-free relaxor ferroelectrics, J. Am. Ceram. Soc. 95 (2012) 1–26.
[78] W. Dmowski, S.B. Vakhrushev, I.K. Jeong, M.P. Hehlen, F. Trouw, T. Egami, Local lattice dynamics and the origin of the relaxor ferroelectric behavior, Phys. Rev. Lett. 100 (2008), 137602.
[79] F. Li, S. Zhang, T. Yang, Z. Xu, N. Zhang, G. Liu, J. Wang, J. Wang, Z. Cheng, Z.-G. Ye, J. Luo, T.R. Shrout, L.-Q. Chen, The origin of ultrahigh piezoelectricity in relaxor-ferroelectric solid solution crystals, Nat. Commun. 7 (2016) 13807.
[80] F. Li, D. Lin, Z. Chen, Z. Cheng, J. Wang, C. Li, Z. Xu, Q. Huang, X. Liao, L.-Q. Chen, T.R. Shrout, S. Zhang, Ultrahigh piezoelectricity in ferroelectric ceramics by design, Nat. Mater. 17 (2018) 349–354.
[81] I. Katsouras, K. Asadi, M. Li, T.B. van Driel, K.S. Kjaer, D. Zhao, T. Lenz, Y. Gu, P. W.M. Blom, D. Damjanovic, M.M. Nielsen, D.M. de Leeuw, The negative piezoelectric effect of the ferroelectric polymer poly(vinylidene fluoride), Nat. Mater. 15 (2016) 78–84.
[82] V. Sencadas, R. Gregorio, S. Lanceros-Mendez, Alpha to beta phase transformation and microestructural changes of PVDF films induced by uniaxial stretch, J. Macromol. Sci. Part B-Phys. 48 (2009) 514–525.
[83] N. Meng, X. Ren, G. Santagiuliana, L. Ventura, H. Zhang, J. Wu, H. Yan, M. J. Reece, E. Bilotti, Ultrahigh β-phase content poly(vinylidene fluoride) with relaxor-like ferroelectricity for high energy density capacitors, Nat. Commun. 10 (2019) 4535.
[84] J.S. Andrew, D.R. Clarke, Effect of electrospinning on the ferroelectric phase content of polyvinylidene difluoride fibers, Langmuir 24 (2008) 670–672.
[85] A. Baji, Y.W. Mai, Q. Li, Y. Liu, Electrospinning induced ferroelectricity in poly (vinylidene fluoride) fibers, Nanoscale 3 (2011) 3068–3071.
[86] T.B. Xu, Z.Y. Cheng, Q.M. Zhang, High-performance micromachined unimorph actuators based on electrostrictive poly(vinylidene fluoride-trifluoroethylene) copolymer, Appl. Phys. Lett. 80 (2002) 1082–1084.
[87] Q.M. Zhang, V. Bharti, X. Zhao, Giant electrostriction and relaxor ferroelectric behavior in electron-irradiated poly(vinylidene fluoride-trifluoroethylene) copolymer, Science 280 (1998) 2101–2104.
[88] X.J. He, K. Yao, B.K. Gan, Phase transition and properties of a ferroelectric poly (vinylidene fluoride-hexafluoropropylene) copolymer, J. Appl. Phys. 97 (2005), 084101.
[89] Y. Liu, B. Zhang, W. Xu, A. Haibibu, Z. Han, W. Lu, J. Bernholc, Q. Wang, Chirality-induced relaxor properties in ferroelectric polymers, Nat. Mater. 19 (2020) 1169–1174.
[90] Y.J. Park, S.J. Kang, B. Lotz, M. Brinkmann, A. Thierry, K.J. Kim, C. Park, Ordered ferroelectric PVDF−TrFE thin films by high throughput epitaxy for nonvolatile polymer memory, Macromolecules 41 (2008) 8648–8654.
[91] H.J. Jung, J. Chang, Y.J. Park, S.J. Kang, B. Lotz, J. Huh, C. Park, Shear-induced ordering of ferroelectric crystals in spin-coated thin poly(vinylidene fluoride-co-trifluoroethylene) films, Macromolecules 42 (2009) 4148–4154.
[92] S.-W. Hahm, D. Kim, D.-Y. Khang, One-dimensional confinement in crystallization of P(VDF-TrFE) thin films with transfer-printed metal electrode, Polymer 55 (2014) 175–181.
[93] S. Chen, K. Yao, F.E.H. Tay, L.L.S. Chew, Comparative investigation of the structure and properties of ferroelectric poly(vinylidene fluoride) and poly (vinylidene fluoride-trifluoroethylene) thin films crystallized on substrates, J. Appl. Polym. Sci. 116 (2010) 3331–3337.
[94] N. Levi, R. Czerw, S.Y. Xing, P. Iyer, D.L. Carroll, Properties of polyvinylidene difluoride-carbon nanotube blends, Nano Lett. 4 (2004) 1267–1271.
[95] S. Manna, A.K. Nandi, Piezoelectric beta polymorph in poly(vinylidene fluoride)-functionalized multiwalled carbon nanotube nanocomposite films, J. Phys. Chem. C. 111 (2007) 14670–14680.
[96] S. Jiang, H. Wan, H. Liu, Y. Zeng, J. Liu, Y. Wu, G. Zhang, High beta phase content in PVDF/CoFe2O4 nanocomposites induced by DC magnetic fields, Appl. Phys. Lett. 109 (2016) 154–158.
[97] Y. Wu, S.L. Hsu, C. Honeker, D.J. Bravet, D.S. Williams, The role of surface charge of nucleation agents on the crystallization behavior of poly(vinylidene fluoride), J. Phys. Chem. B 116 (2012) 7379–7388.
[98] K.-I. Park, M. Lee, Y. Liu, S. Moon, G.-T. Hwang, G. Zhu, J.E. Kim, S.O. Kim, D. K. Kim, Z.L. Wang, K.J. Lee, Flexible nanocomposite generator made of BaTiO3 nanoparticles and graphitic carbons, Adv. Mater. 24 (2012) 2999–3004.
[99] C.K. Jeong, K.-I. Park, J. Ryu, G.-T. Hwang, K.J. Lee, Large-area and flexible lead-free nanocomposite generator using alkaline niobate particles and metal nanorod filler, Adv. Funct. Mater. 24 (2014) 2620–2629.
[100] M. Xie, Y. Zhang, M.J. Kraśny, C. Bowen, H. Khanbareh, N. Gathercole, Flexible and active self-powered pressure, shear sensors based on freeze casting ceramic–polymer composites, Energy Environ. Sci. 11 (2018) 2919–2927.
[101] H. Liu, X. Lin, S. Zhang, Y. Huan, S. Huang, X. Cheng, Enhanced performance of piezoelectric composite nanogenerator based on gradient porous PZT ceramic structure for energy harvesting, J. Mater. Chem. A 8 (2020) 19631–19640.
[102] H.L. Cox, The elasticity and strength of paper and other fibrous materials, British, J. Appl. Phys. 3 (1952) 72–79.
[103] B.A. Newcomb, H.G. Chae, P.V. Gulgunje, K. Gupta, Y. Liu, D.E. Tsentalovich, M. Pasquali, S. Kumar, Stress transfer in polyacrylonitrile/carbon nanotube composite fibers, Polymer 55 (2014) 2734–2743.
[104] C. Hu, L. Cheng, Z. Wang, Y. Zheng, S. Bai, Y. Qin, A transparent antipeep piezoelectric nanogenerator to harvest tapping energy on screen, Small 12 (2016) 1315–1321.
[105] M. Zhang, T. Gao, J. Wang, J. Liao, Y. Qiu, H. Xue, Z. Shi, Z. Xiong, L. Chen, Single BaTiO3 nanowires-polymer fiber based nanogenerator, Nano Energy 11 (2015) 510–517.
[106] Z. Chen, X. Song, L. Lei, X. Chen, C. Fei, C.T. Chiu, X. Qian, T. Ma, Y. Yang, K. Shung, Y. Chen, Q. Zhou, 3D printing of piezoelectric element for energy focusing and ultrasonic sensing, Nano Energy 27 (2016) 78–86.
[107] H. Cui, R. Hensleigh, D. Yao, D. Maurya, P. Kumar, M.G. Kang, S. Priya, X. Zheng, Three-dimensional printing of piezoelectric materials with designed anisotropy and directional response, Nat. Mater. 18 (2019) 234–241.
[108] J. Li, Y. Long, F. Yang, H. Wei, Z. Zhang, Y. Wang, J. Wang, C. Li, C. Carlos, Y. Dong, Y. Wu, W. Cai, X. Wang, Multifunctional artificial artery from direct 3D printing with built-in ferroelectricity and tissue-matching modulus for real-time sensing and occlusion monitoring, Adv. Funct. Mater. 30 (2020), 2002868.
[109] G. Zhang, D. Brannum, D. Dong, L. Tang, E. Allahyarov, S. Tang, K. Kodweis, J.-K. Lee, L. Zhu, Interfacial polarization-induced loss mechanisms in polypropylene/BaTiO3 nanocomposite dielectrics, Chem. Mater. 28 (2016) 4646–4660.
[110] H. Ueda, E. Fukada, F.E. Karasz, Piezoelectricity in three-phase systems: effect of the boundary phase, J. Appl. Phys. 60 (1986) 2672–2677.
[111] J. Liu, P. Fei, J.H. Song, X.D. Wang, C.S. Lao, R. Tummala, Z.L. Wang, Carrier density and Schottky barrier on the performance of DC nanogenerator, Nano Lett. 8 (2008) 328–332.
[112] K.Y. Lee, B. Kumar, J.-S. Seo, K.-H. Kim, J.I. Sohn, S.N. Cha, D. Choi, Z.L. Wang, S.-W. Kim, P-type polymer-hybridized high-performance piezoelectric nanogenerators, Nano Lett. 12 (2012) 1959–1964.
[113] A. Dal Corso, M. Posternak, R. Resta, A. Baldereschi, Ab initio study of piezoelectricity and spontaneous polarization in ZnO, Phys. Rev. B 50 (1994) 10715–10721.
[114] D. Karanth, H. Fu, Large electromechanical response in ZnO and its microscopic origin, Phys. Rev. B 72 (2005), 064116.
[115] J.T. Luo, Y.C. Yang, X.Y. Zhu, G. Chen, F. Zeng, F. Pan, Enhanced electromechanical response of Fe-doped ZnO films by modulating the chemical state and ionic size of the Fe dopant, Phys. Rev. B 82 (2010), 014116.
[116] Y. Zhang, C. Liu, J. Liu, J. Xiong, J. Liu, K. Zhang, Y. Liu, M. Peng, A. Yu, A. Zhang, Y. Zhang, Z. Wang, J. Zhai, Z.L. Wang, Lattice strain induced remarkable enhancement in piezoelectric performance of ZnO-based flexible nanogenerators, ACS Appl. Mater. Interfaces 8 (2016) 1381–1387.
[117] H.J. Choi, Y.S. Jung, J. Han, Y.S. Cho, In-situ stretching strain-driven high piezoelectricity and enhanced electromechanical energy-harvesting performance of a ZnO nanorod-array structure, Nano Energy 72 (2020), 104735.
[118] H. Kim, S. Yun, K. Kim, W. Kim, J. Ryu, H.G. Nam, S.M. Han, S. Jeon, S. Hong, Breaking the elastic limit of piezoelectric ceramics using nanostructures: a case study using ZnO, Nano Energy 78 (2020), 105259.
[119] X. Wang, J. Song, J. Liu, Z.L. Wang, Direct-current nanogenerator driven by ultrasonic waves, Science 316 (2007) 102–105.
[120] Y. Qin, X. Wang, Z.L. Wang, Microfibre-nanowire hybrid structure for energy scavenging, Nature 451 (2008) 809–813.
[121] R. Yang, Y. Qin, L. Dai, Z.L. Wang, Power generation with laterally packaged piezoelectric fine wires, Nat. Nanotechnol. 4 (2009) 34–39.
[122] S. Xu, Y. Qin, C. Xu, Y. Wei, R. Yang, Z.L. Wang, Self-powered nanowire devices, Nat. Nanotechnol. 5 (2010) 366–373.
[123] M. Riaz, J. Song, O. Nur, Z.L. Wang, M. Willander, Study of the Piezoelectric Power Generation of ZnO Nanowire Arrays Grown by Different Methods, Adv. Funct. Mater. 21 (2011) 628–633.
[124] G. Zhu, R. Yang, S. Wang, Z.L. Wang, Flexible high-output nanogenerator based on lateral ZnO nanowire array, Nano Lett. 10 (2010) 3151–3155.
[125] Y. Hu, L. Lin, Y. Zhang, Z.L. Wang, Replacing a battery by a nanogenerator with 20 V output, Adv. Mater. 24 (2012) 110–114.
[126] G. Zhu, A.C. Wang, Y. Liu, Y.S. Zhou, Z.L. Wang, Functional electrical stimulation by nanogenerator with 58 v output voltage, Nano Lett. 12 (2012) 3086–3090.
[127] T.P. Lei, Z.J. Xu, X.M. Cai, L. Xu, D.H. Sun, New insight into gap electrospinning: toward meter-long aligned nanofibers, Langmuir 34 (2018) 13788–13793.
[128] W. Wu, S. Bai, M. Yuan, Y. Qin, Z.L. Wang, T. Jing, Lead zirconate titanate nanowire textile nanogenerator for wearable energy-harvesting and self-powered devices, Acs Nano 6 (2012) 6231–6235.
[129] K.-I. Park, J.H. Son, G.-T. Hwang, C.K. Jeong, J. Ryu, M. Koo, I. Choi, S.H. Lee, M. Byun, Z.L. Wang, K.J. Lee, Highly-efficient, flexible piezoelectric PZT thin film nanogenerator on plastic substrates, Adv. Mater. 26 (2014) 2514–2520.

[130] L. Gu, J. Liu, N. Cui, Q. Xu, T. Du, L. Zhang, Z. Wang, C. Long, Y. Qin, Enhancing the current density of a piezoelectric nanogenerator using a three-dimensional intercalation electrode, Nat. Commun. 11 (2020) 1030.
[131] Y.K. Ramadass, A.P. Chandrakasan, An efficient piezoelectric energy harvesting interface circuit using a bias-flip rectifier and shared inductor, IEEE J. Solid-State Circuits 45 (2010) 189–204.
[132] M.B. Khan, D.H. Kim, J.H. Han, H. Saif, H. Lee, Y. Lee, M. Kim, E. Jang, S.K. Hong, D.J. Joe, T.-I. Lee, T.-S. Kim, K.J. Lee, Y. Lee, Performance improvement of flexible piezoelectric energy harvester for irregular human motion with energy extraction enhancement circuit, Nano Energy 58 (2019) 211–219.
[133] Y. Gao, Z.L. Wang, Equilibrium potential of free charge carriers in a bent piezoelectric semiconductive nanowire, Nano Lett. 9 (2009) 1103–1110.
[134] D. Hu, M. Yao, Y. Fan, C. Ma, M. Fan, M. Liu, Strategies to achieve high performance piezoelectric nanogenerators, Nano Energy 55 (2019) 288–304.

Qi Xu received his B.S and Ph.D from the School of Physical Science and Technology of Lanzhou University in 2010 and 2017, respectively. Currently, he is an assistant professor at the Institute of Nanoscience and Nanotechnology, Lanzhou University, China. His research focused on self-powered systems and high performance UV sensors.

Juan Wen received her B.S (2006) in Material Physics and Ph. D (2016) in Particle Physics and Nuclear Physics from Lanzhou University. From 2014–2016, she studied as a joint Ph.D student at Los Alamos National Laboratory (LANL) in the USA. Currently, she is an assistant professor at the Institute of Nanoscience and Nanotechnology, Lanzhou University, China. Her research focused on nanoenergy technology, self-powered systems and nuclear materials.

Yong Qin received his B.S. (1999) in Material Physics and Ph. D. (2004) in Material Physics and Chemistry from Lanzhou University. From 2007–2009, he worked as a visiting scholar and Postdoc in Professor Zhong Lin Wang's group at Georgia Institute of Technology. Currently, he is a professor at the Institute of Nanoscience and Nanotechnology, Lanzhou University, where he holds a Cheung Kong Chair Professorship. His research interests include nanoenergy technology, functional nanodevice and self-powered nanosystem. Details can be found at: http://www.yqin.lzu.edu.cn.